

PAPER

Electrical properties of tissues from a microscopic model of confined electrolytes

To cite this article: Francisco J Solis and Vikram Jadhao 2023 Phys. Med. Biol. 68 105017

View the article online for updates and enhancements.

You may also like

- Characterization and development of an electrical conductivity flow cell for the axial continuous phase fraction profiling of bulk multiphase flow
 M R Lepage, L Vinnett, C O Gomez et al.
- Enhanced ionic conductivity in LAGP/LATP composite electrolyte Shi-Gang Ling, , Jia-Yue Peng et al.
- Investigation of proton conductivity in Sc and Yb co-doped barium zirconate

Avishek Satapathy, Ela Sinha and S K Rout



Physics in Medicine & Biology





RECEIVED 15 October 2022

REVISED 16 February 2023

ACCEPTED FOR PUBLICATION

21 April 2023

PUBLISHED 15 May 2023

PAPER

Electrical properties of tissues from a microscopic model of confined electrolytes

Francisco J Solis^{1,*} o and Vikram Jadhao²

- 1 School of Mathematical and Natural Sciences, Arizona State University, Glendale, AZ 85306, United States of America
- ² Intelligent Systems Engineering, Indiana University, Bloomington, IN 47408, United States of America
- Author to whom any correspondence should be addressed.

E-mail: francisco.solis@asu.edu and vjadhao@iu.edu

Keywords: tissue properties, tissue impedance, electric response

Abstract

Objective. In the presence of oscillatory electric fields, the motion of electrolyte ions in biological tissues is often limited by the confinement created by cell and organelle walls. This confinement induces the organization of the ions into dynamic double layers. This work determines the contribution of these double layers to the bulk conductivity and permittivity of tissues. *Approach*. Tissues are modeled as repeated units of electrolyte regions separated by dielectric walls. Within the electrolyte regions, a coarse-grained model is used to describe the associated ionic charge distribution. The model emphasizes the role of the displacement current in addition to the ionic current and enables the evaluation of macroscopic conductivities and permittivities. Main results. We obtain analytical expressions for the bulk conductivity and permittivity as a function of the frequency of the oscillatory electric field. These expressions explicitly include the geometric information of the repeated structure and the contribution of the dynamic double layers. The low-frequency limit of the conductivity expression yields a result predicted by the Debye permittivity form. The model also provides a microscopic interpretation of the Maxwell–Wagner effect. Significance. The results obtained contribute to the interpretation of the macroscopic measurements of electrical properties of tissues in terms of their microscopic structure. The model enables a critical assessment of the justification for the use of macroscopic models to analyze the transmission of electrical signals through tissues.

1. Introduction

The macroscopic response of biological tissues to externally applied or internally generated electric impulses can provide important information regarding the internal tissue structure. Characterizing this response is useful in the design of materials relevant to medical applications and human-machine interfaces (Nunez *et al* 2006, Grimnes and Martinsen 2011, Makarov *et al* 2015). As a characterization tool, conductivity measurements have been shown to differentiate between tissues in different states and thus serve as potential diagnostic tools. For example, the conductivities of some cancerous tissues have been shown to differ from those of healthy tissues (Åberg *et al* 2011, Grenier *et al* 2013, Braun *et al* 2017, Teixeira *et al* 2018). Electrical properties can also differentiate between different life stages of organisms (Grossi and Riccò 2017, Flores-Cosío *et al* 2020, Ibba *et al* 2021). Tissue conduction is also relevant to the interpretation of biological signals such as those observable in electroencephalographic (EEG) recordings. The inverse problem that aims to localize the origin of EEG signals in response to a physiological stimulus relies on modeling the human head as a set of conducting media (Geselowitz 1967, Mosher *et al* 1999, Nunez *et al* 2006, Grech *et al* 2008, Solis and Papandreou-Suppappola 2019). Typical models consider the head composed of homogeneous materials characterized with parameters usually obtained from animal studies. In yet another direction, we note that human-body-mediated signal transmission requires modeling of electrical conduction in tissues (Swaminathan *et al* 2015, Wang *et al* 2015,

Lodi et al 2020). In all these areas, a conceptual link between the microscopic model parameters used to describe the cell-level or tissue-level structure and macroscopic electrical properties is important to make further progress. We note that microscopic-level multicompartment models have been successfully applied to understand cells in solution and interpret the properties of some vegetable tissues (Schwan 1957, Takashima et al 1989, Kuang and Nelson 1997, 1998, Angersbach et al 1999, Grossi and Riccò 2017). Further, it is important to note that similar questions arise in non-biological contexts, e.g. in electrolyte-based soft materials for energy and separation applications, where understanding the link between microscopic structure and macroscopic properties is useful (Sareni et al 1996, Brosseau 2006, Wang and Pan 2008, Jing et al 2015, Zhang et al 2018, Faucher et al 2019, Zhbanov and Yang 2020).

For oscillating external fields of frequency ω , the response of the macroscopic samples can be described by means of a frequency-dependent complex conductivity $\sigma(\omega)$ or permittivity $\varepsilon(\omega)$. These quantities exhibit distinct regimes characterized by drops in the values of the real part of the permittivity accompanied by the appearance of peaks in its imaginary part (Foster et al 1986, Takashima et al 1989, Kuang and Nelson 1998, Grimnes and Martinsen 2011). Considerable variations in peak location and width across materials is observed (Gabriel et al 1996a, 1996b, 1996, 2009).

For frequencies in the GHz range, the response is dominated by molecular-level polarization and classified as belonging to the γ -dispersion regime. In the MHz range, peaks in the imaginary part of the permittivity of cell suspensions are well understood as arising from the contrast between the electrical properties of the cells and their suspension medium. Features in this range appear in many types of tissues and systems and are classified as belonging to the β -dispersion regime. Finally, the α -dispersion regime refers to a similar type of response that appears at frequencies in the kHz region or below, though its origin is less well understood (Foster et al 1986, Takashima et al 1989, Kuang and Nelson 1998, Martinsen et al 1998, Grimnes et al 2002, Gabriel et al 2009, Abdalla 2011, Grimnes and Martinsen 2011, Nordbotten et al 2014, Podtaev et al 2015, Crowell et al 2020, Bouchaala et al 2021).

Many previous studies have used a bulk macroscopic model for the description of currents in confined regions. We note that a confined electrolyte, in the presence of oscillating external fields, accumulates ions on the confining boundaries and creates *dynamic double layers*. The role of these ionic double layers have been considered in some detail in the exterior of cells in solution by modeling the cells as colloidal particles (Grosse and Schwan 1992) and examining dispersion in the colloidal suspension (Schwarz 1962, Dukhin et al 1974, Grosse and Delgado 2010). Here, we consider currents and the double layers inside the cells confined by dielectric walls inaccessible to ions. We develop a microscopic model comprising a sequence of regions of confined electrolytes separated by dielectric walls, that explicitly considers the effects of the external electric field and the dielectric discontinuities at the electrolyte-wall interfaces on the formation of double layers. It is assumed that the confining walls are themselves uncharged and hydrodynamic effects are ignored.

A sketch of the microscopic model system considered appears in figure 1. It contains an electrolyte region (cell interior) of size $L_{\rm E}$ confined by thin dielectric walls (cell walls and cell exterior) of thickness $L_{\rm D}$, and an electric field in the direction perpendicular to the walls. Our key result is an analytical expression for the conductivity of this system. In section 3.3, we arrive at the result

$$\sigma(\omega) = \frac{\omega}{\omega - i\Omega(\omega)} \sigma^{E}(\omega), \tag{1}$$

where $i = \sqrt{-1}$ represents the unit imaginary number, and the characteristic parameters $\Omega(\omega)$ and $\sigma^{\rm E}(\omega)$ are complex and have a frequency dependence. At low frequencies, both these parameters have real limits Ω_0 and σ_0^E . The first, Ω_0 , has units of frequency and can be interpreted as the inverse of the characteristic relaxation time associated with the double layer buildup process. The second, $\sigma_0^{\rm E}$, captures the conductivity of the pure electrolyteregion. Our key result has a low-frequency ($\omega \ll \Omega_0$) limit of the form: $\sigma(\omega) \approx \frac{\omega}{\omega - i\Omega_0} \sigma_0^{\rm E}.$

$$\sigma(\omega) \approx \frac{\omega}{\omega - i\Omega_0} \sigma_0^{\rm E}.$$
 (2)

Most discussions of electric properties of tissues under oscillating fields consider the Debye form of the complex permittivity which is the sum over the terms $\Delta \varepsilon/(1+i\tau\omega)$, where $\Delta \varepsilon$ and τ represent an excess permittivity contribution and its associated relaxation time respectively (Hurt 1985, Foster et al 1986, Gabriel et al 1996a, Eleiwa and Elsherbeni 2001). These terms lead to conductivity contributions of the form $\sigma(\omega) = \omega \tau \Delta \varepsilon / (\omega - i\tau^{-1})$. We refer to this form as a Debye-type conductivity, and show that the low frequency limit of our main result, equation (1), has this Debye form.

The new expression for the variation of conductivity and permittivity with frequency enables a closer examination of the link between the material heterogeneities and phenomena in the α and β -dispersion regimes. The dynamic double layers in the interior of cells have a characteristic size given by the screening length $\kappa^$ associated with the electrolyte solution that emerges from ionic interactions (Kilic et al 2007a, Israelachvili 2011). As shown below, several features of the response result directly from the double layers, and

Figure 1. The top panel shows a set of similar electrolyte regions (white) separated by thick dielectric walls (gray) impermeable to ions. The bottom panel shows the simplified one-dimensional periodic structure used for model calculations with a horizontal electric field (solid field lines). The walls parallel to the field are ignored in the model. All electrolyte regions have size $L_{\rm E}$ and all walls have thickness $L_{\rm D}$. The horizontal axis is represented using the Cartesian coordinate x with the origin at the mid point of an electrolyte region.

both dimensionless quantities: the ratio of the wall thickness and the electrolyte-region thickness (L_D/L_E) and κL_E , determine the relaxation times characterizing the conductivity at low frequencies.

An important part of the discussion presented addresses the role of ionic currents. In the bulk of the electrolyte regions, these currents form the main component of the total net current, which also includes a relatively smaller contribution from the displacement current (Scott *et al* 2000a, 2000b, Barbero and Alexe-Ionescu 2005). The net current, which we also refer to as the electromagnetic current, is conserved throughout the material. That is, as a vector field it is divergenceless This is the case even when ions are completely blocked in the wall region, where the displacement current dominates (Eisenberg *et al* 2017, Eisenberg 2018). The explicit description of charge distributions and currents, including displacement currents within the dielectric walls, leads to refined interpretations of experimental measurements of tissue properties and clearer understanding of tissue-related phenomena such as the Maxwell–Wagner effect. Further, our work signals the need to reconsider some macroscopic models comm employed to examine the electrical properties of tissues.

The rest of the paper is organized as follows. The current contributions and macroscopic description are presented in section 2. The microscopic model is introduced in detail in section 3, which also provides expressions for the conductivity and permittivity. Section 4 presents the results associated with several illustrative examples. Section 5 discusses the connections of the microscopic model with experimental measurements and the Maxwell–Wagner effect, and presents conclusions.

2. Macroscopic description of currents in tissues

The analysis of electrical phenomena in biological systems uses methods and models where alternating currents (AC) as well as direct currents (DC) are relevant. Macroscopic tissue properties are often characterized by AC impedances. On the other hand, description of electroencephalographic (EEG) signals assumes quasi-static currents characterized by DC properties. Though related, the currents in these contexts are not the same. In DC or quasi-static systems, the current is the flow of charged particles. In AC systems, this definition is modified to include a displacement current term that allows a seamless description of capacitive and inductive components, so that the newly defined current is conserved within circuits.

As in the examples noted above, context dictates the meaning of the current but, in some cases, an explicit distinction is required. This article focuses on AC properties in regimes where ionic flux is relevant, typically below 1 GHz, when molecular polarization is more prominent. The presence of the ionic flux component of the current demands a careful choice of nomenclature. In addition, the explicit use of the concepts of the displacement and electromagnetic currents introduced below, makes the discussion more precise and insightful. The electromagnetic current has two key properties. First, it is fundamentally conserved due to the structure of Maxwell's equations. Second, in the complex domain, it is the object that satisfies a generalized constitutive equation relating current and electric field, and thus defines the complex conductivity.

The explicit definitions of the different currents are as follows. The flux of unbound charged particles defines a current density \mathbf{j} . The displacement current density \mathbf{j}_D in a medium can be defined as the time derivative of the displacement field \mathbf{D} :

$$\mathbf{j}_{\mathrm{D}} = \partial_t \mathbf{D}. \tag{3}$$

In linear materials this is proportional to the electric field \mathbf{E} , $\mathbf{D} = \varepsilon_0 \varepsilon \mathbf{E}$ with ε_0 and ε are the vacuum and medium permittivity respectively. The sum of the particle and displacement current densities is the object that appears in Maxwell's equations. It is referred here as the electromagnetic current density \mathbf{J} :

$$J = j + j_{D}. \tag{4}$$

Moving forward, we will refer to \mathbf{j} , \mathbf{j}_d , and \mathbf{J} as simply particle, displacement, and electromagnetic currents respectively. When the particles are ions, the term ionic current is used. In the one-dimensional (1D) case the current densities (fluxes) are proportional to currents through a fixed cross-sectional area perpendicular to the flow direction.

In AC systems, the electromagnetic current **J** coincides with the circuit current (Harrington *et al* 1961, Fano *et al* 1963, Jackson 1999). The current **J** is divergenceless:

$$\nabla \cdot \mathbf{J} = 0. \tag{5}$$

In other words, the electromagnetic current is conserved. Gauss' law equates the divergence of the electric displacement vector in a medium with the charge density ρ of free particles: $\nabla \cdot \mathbf{D} = \varepsilon_0 \nabla \cdot \varepsilon \mathbf{E} = \rho$. Therefore, the zero divergence of the electromagnetic current can be interpreted as a continuity equation:

$$\nabla \cdot \mathbf{J} = \partial_t \rho + \nabla \cdot \mathbf{j} = 0. \tag{6}$$

While the ionic current is of fundamental interest, the current measurements in electrical circuits correspond directly to the electromagnetic current. For example, a simple Ammeter detects the magnetic field **B** created by a circuit. Its value is determined from Ampere's and Faraday's laws and it turns out to be linear in the electromagnetic current **J**, rather than in the flux of charged particles **j**. Previous studies have emphasized the need to have a clear distinction between **j** and **J** (Fuller and Ward 1970), and have highlighted the key role of the displacement current in the description of microscopic processes in heterogeneous materials (Eisenberg *et al* 2017, Eisenberg 2018).

The divergenceless condition, equation (5) is true for the current expressed as a function of time and position as well as in the frequency domain. In the latter case, it is standard to consider a single frequency ω , in which case we write $J(t) = Re[J(\omega)e^{i\omega t}]$, where $Re[\cdot]$ denotes the real part of the argument and $J(\omega)$ is a frequency-dependent, complex amplitude. The conservation of the electromagnetic current in the time domain immediately implies the conservation of $J(\omega)$ in the frequency domain.

For a two terminal circuit element with external oscillating sources and linear elements, the impedance $Z = V(\omega)/I(\omega)$ is defined as the ratio of the amplitude of the potential drop $V(\omega)$ to the circuit current $I(\omega)$. A definition for more general systems is based on the rate of energy dissipation in a space region, though this will not be needed in this article (Harrington *et al* 1961, Fano *et al* 1963, Jackson 1999). In a homogeneous, passive element of length L and cross-section area A, a *complex* conductivity can be defined as $\sigma(\omega) = L/(ZA)$. This definition makes sense for macroscopic objects as long as the local behavior can be averaged. In the case of tissues, $\sigma(\omega)$ characterizes an average over many cells. Noting that the magnitude of the potential drop in the element can be expressed as $E_{av}L$, where E_{av} is the complex amplitude of an average electric field, the definition of the complex conductivity implies the following linear constitutive relation:

$$\mathbf{J}(\omega) = \sigma(\omega)\mathbf{E}_{av}(\omega). \tag{7}$$

It must be emphasized that this linear relation works in the frequency domain, and that J is the electromagnetic (or circuit) current. The field \mathbf{E}_{av} is an average over the microscopic values of the electric field, which is simply denoted by \mathbf{E} .

The structure of the different currents in the context of bounded electrolytes is sketched in figure 2. Two neighboring regions with ions are separated by a hard wall. An oscillatory external electric field is applied in the horizontal direction. In the bulk of the electrolyte regions, far away from the walls, the combination of the external field and local contributions due to the small accumulation of charges still produce a net field in the same direction as the external one. There, the ionic current ${\bf j}$ satisfies the constitutive equation ${\bf j}=\sigma_0{\bf E}$, with σ_0 being the conductivity of the ionic medium. In the bulk region, there are no significant charge density gradients that contribute to the creation of ionic currents. The electromagnetic current in this region is ${\bf J}=\sigma_0{\bf E}+\varepsilon_E\varepsilon_0\partial_t{\bf E}$, where it is assumed that the local permittivity ε_E is that of water ($\varepsilon_E=80$). The bulk electrolyte has a characteristic frequency $\Omega_E=\sigma_0/\varepsilon_E\varepsilon_0$, typically in the range of GHz. In the bulk region of a pure electrolyte at frequencies much lower than Ω_E , the electromagnetic current and the ionic current approximately coincide, ${\bf J}\approx{\bf j}_{\rm Bulk}$.

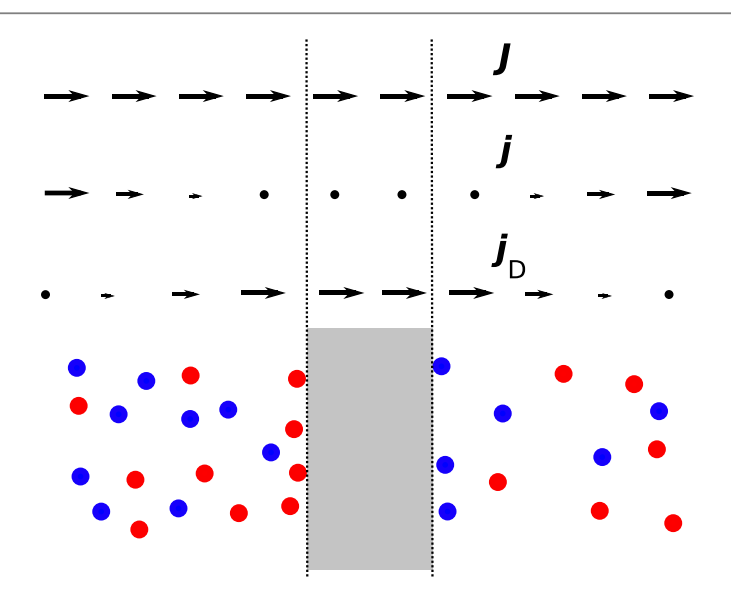


Figure 2. Structure of currents near an impermeable wall in an effective one-dimensional system. The left and right electrolyteregions are separated by a dielectric wall shown in gray. Electrolyte ions in solution are shown as circles. The extreme left and right edges of the figure are considered to have the bulk properties of the respective electrolyte regions. The two electrolyteregions can have different ionic densities. The electromagnetic current \mathbf{J} , at top, is spatially constant. Below, the ionic current \mathbf{j} has equal bulk value in both electrolyteregions, but decays to zero near the dielectric wall. In the third row, the displacement current \mathbf{j}_D is large inside the dielectric wall and small in the electrolyteregions, where it reflects the dynamic changes in the accumulated charge near the wall and thus in the electric displacement field. See also figure 3 for a numerical example.

The figure also shows the presence of two double layers, one at each side of the wall. These double-layers are dynamic and appear due to the stopped flux of ions at the wall. In contrast to the bulk region, changes in the charge density in this region produce non-negligible contributions to the displacement current. Inside the hard wall region there is no ionic current $\mathbf{j} = \mathbf{0}$ and the total current equals the displacement current $\mathbf{J} = \mathbf{j}_D$. The region is permeated by the time-varying electric field. In the 1D case, the electric field must be spatially uniform because its divergence is zero inside the dielectric wall region. In tissues, the field in the walls connects the electrical activity across the electrolyteregions.

In the situation sketched in the figure, the two compartments separated by the wall do not have the same properties; the sketch suggests different ionic concentrations. The ionic conductivities of these two compartments are thus different. The previous analysis shows, however, that in a 1D geometry, the two compartments have identical electromagnetic current at all times for any frequency, and a nearly equal ionic current in their bulk at low frequencies because the total current is mainly conductive in this region. In short, in spite of the presence of a hard wall, where it is actually zero, the ionic current is essentially continuous at low frequencies. These characteristics appear in the numerical examples presented below. We also note similar discussions in (Eisenberg *et al* 2017).

It is worth noticing that the previous discussion carries over to tissues in contact with an electrode. Away form the actual electrode contact, the circuit current in the measuring device can be identified with the flux of electrons, and is approximately equal to the ionic current in the most conducting regions of the tissue. On the other hand, it should also be stressed that the macroscopic calculations of conductivity and impedance must use the full electromagnetic current.

3. Microscopic model of tissues based on confined electrolytes

We consider the setup shown in figure 1 where, in the direction of an applied external electric field, the tissue can be considered as a set of similar electrolyteregions separated by thick dielectric walls. The transversal size of the regions is not crucial to the analysis and thus we consider an effective 1D model. The electrolyteregion has length $L_{\rm E}$ and the dielectric wall has thickness $L_{\rm D}$. The repeated structure has a total length of $L=L_{\rm E}+L_{\rm D}$. It is useful to define the length ratios: $\ell_{\rm E}=L_{\rm E}/L$ and $\ell_{\rm D}=L_{\rm D}/L$. We adopt a system of coordinates where the variable x is aligned with the field, the origin is at the center of an electrolyteregion, and the centers of the dielectric walls are at $\pm L/2$, $\pm 3L/2$,

The properties of the confined electrolyte can be discussed by adopting a coarse-grained representation where average values of the ionic distribution and charge densities make sense. It is assumed that the electrolyteregion is overall electroneutral and contains a monovalent (1:1) electrolyte. Both charged species

(cations and anions) have equal number densities n_0 . In the electrolyteregion, the model becomes a well-studied system for diffusion in the presence of electric fields (Buck 1969, MaCdonald 1970, Macdonald *et al* 1987, Bazant *et al* 2004). A description of the ionic currents, potential and impedance are presented for a similar model in previous works (Cirkel *et al* 1997, Scott *et al* 2000a, 2000b, Barbero and Alexe-Ionescu 2005). The derivation below aims at setting these results in the context of tissues and extending them by explicitly considering the properties of the ionic, displacement and electromagnetic currents, and by taking into account the microscopic structure of the dynamic double layers. Related models have been studied for other geometries, focusing on single cells or cell suspensions (Schwarz 1962, Dukhin *et al* 1974, Foster *et al* 1986, Dukhin *et al* 1999, Koch 2004, Grosse and Delgado 2010). Tissues have been less explored, and often modeled as sequences of slabs of homogeneous materials. A connection between the properties of these slabs and the underlying microscopic structure is not established (Kuang and Nelson 1998, Grimnes and Martinsen 2011).

3.1. Electrolyte region

The motion of individual ions in the confined electrolyteregion leads to changes in the local charge density ρ as a function of space and time. The flux of ions of a given charged species s (e.g. monovalent cations) is dictated by the dissipative dynamics driven by the gradient of the electrochemical potential μ_s characterizing the species. The average velocity \mathbf{v}_s of a group of ions associated with species s is given by

$$\mathbf{v}_{s} = -\gamma \nabla \mu_{s},\tag{8}$$

where γ is the ion mobility. While γ generally depends on the ionic attributes (e.g. size, valency), we will assume ions of both charged species to have the same mobilities. This model applies to ions in solution that are free. When ions are associated to organelles or other cellular structures their mobility is greatly reduced. We assume that the main contribution to conductivity arises from the free ions, though it is known that surface motion contributes to electric response (Shilov *et al* 2001). In The electrochemical potential μ_s is assumed to be determined by entropic and electrostatic interactions:

$$\mu_{\rm s} = k_{\rm B}T \ln(n_{\rm s}/n_0) + ez_{\rm s}\phi, \tag{9}$$

where the first term is the entropic term given by the product of the Boltzmann constant k_B , the temperature T, and the logarithm of the ratio between the local concentration n_s and the average concentration n_0 of the charged species. The second term is the electrostatic energy obtained via the product of the fundamental charge e, ion valency z_s , and the electrostatic potential ϕ . This potential combines both the effect of the external field and the local mean-field created by the charge density ρ . This chemical potential construction is standard in the context of dynamic ion conduction (Bazant *et al* 2004, Kilic *et al* 2007a).

Noting that the gradient of the electrochemical potential is $\nabla \mu_s = k_B T n_s^{-1} \nabla n_s - e z_s E$, where $\mathbf{E} = -\nabla \phi$ is the local electric field, the local current j_s for species s is obtained as

$$\mathbf{j}_{s} = ez_{s}n_{s}\mathbf{v}_{s} = -ez_{s}\gamma k_{B}T\nabla n_{s} + \gamma e^{2}z_{s}^{2}n_{s}\mathbf{E}. \tag{10}$$

The last term in equation (10) is nonlinear because the local electric field E depends on the particle density n_s . An electrolyte in the absence of an external field has uniform concentration n_0 and zero electric field E. The linearization of the product n_s E around this state is n_0 E. In what follows, this linear approximation is used. The role of nonlinear terms has been discussed for the static case in biological contexts in (Levin 2002) and for general electrolyte systems in (Bazant *et al* 2004, Kilic *et al* 2007a). Limitations are also known from experimental work (Wright 2007). Typical cells and tissues have ionic concentrations in the 100 mM range. At these concentrations, a linear response analysis is possible. Corrections to the linearization approximation appear in electrolyte systems at room temperatures when concentrations of monovalent salts are higher than ~1 M (Bazant *et al* 2004, Kilic *et al* 2007a, 2007b, Israelachvili 2011). While average concentrations in biological systems are often below this regime, ion accumulation in the double layers can reach very high concentrations. The presence of corrections can be determined by comparing the highest predicted concentration with the 1 M threshold value.

Summing the currents in equation (10) over both species, the charge density becomes $\rho = \sum_s ez_s n_s$ and the net ionic current $\mathbf{j} = \sum_s \mathbf{j}_s$ is given by

$$\mathbf{j} = -D\nabla\rho + \sigma_0 \mathbf{E},\tag{11}$$

where D is the diffusion constant:

$$D = \gamma k_{\rm B} T, \tag{12}$$

and σ_0 is the intrinsic conductivity for a 1:1 electrolyte:

$$\sigma_0 = 2\gamma e^2 n_0. \tag{13}$$

Using **j** from equation (11) in equation (6), the continuity equation for the charge density ρ leads to $\partial_t \rho = D\nabla^2 \rho - \sigma_0 \nabla \cdot \mathbf{E}$. Assuming that the electrolyteregion can be modeled as a uniform dielectric medium characterized with a relative permittivity $\varepsilon_{\rm E}$, and using Gauss' law $\nabla \cdot \mathbf{E} = \rho/(\varepsilon_0 \varepsilon_{\rm E})$, one obtains the standard

(Nernst–Planck) transport equation:

$$\partial_t \rho = D[\nabla^2 \rho - \kappa^2 \rho],\tag{14}$$

where κ is the inverse screening length given by $\kappa^2 = \sigma_0/(\varepsilon_0 \varepsilon_E D) = 2e^2 n_0/(\varepsilon_0 \varepsilon_E k_B T)$. From here on, we consider water as the dielectric medium inhabited by the ions.

In addition to solving equation (14), it is necessary to also determine the electric potential ϕ by solving the Poisson equation, and applying the boundary conditions set by the external field \mathbf{E}_{ext} . The Poisson equation is obtained by substituting $\mathbf{E} = -\nabla \phi$ in Gauss's law:

$$-\varepsilon_0 \varepsilon_{\rm E} \nabla^2 \phi = \varepsilon_0 \varepsilon_{\rm E} \nabla \cdot \mathbf{E} = \rho. \tag{15}$$

The boundary conditions for the electrolyteregion considered are: no-particle flux on the confining dielectric walls ($\mathbf{j}|_{wall} = 0$), continuity of the potential, and the matching of electric displacement at the electrolyte-wall interface. In the 1D case, the solutions of the Poisson equation can be written in the form new

$$\phi(x,t) = \phi_c(x,t) - xE_B(t). \tag{16}$$

The first term, ϕ_c is a solution of the Poisson equation (equation (15)) with an inhomogeneous term equal to the accumulated charges ρ . The derivative of ϕ_c is zero at the midpoint of the electrolyte region. The second term $xE_B(t)$ is a spatially-linear potential that solves the homogeneous Poisson equation ($\nabla^2 \phi = 0$) and enables the matching of appropriate boundary conditions. $E_B(t)$ is the time-varying magnitude of a spatially-constant electric field, which can be identified with the total field at the center of the electrolyte. E_B is not the external field because it also has contributions due to the charges in the system outside the immediate electrolyte region.

In the following, unless otherwise noted (e.g. for the electromagnetic current density), we will use the same symbol for the time and frequency domain amplitudes. Inside the electrolyteregion, the ion concentration can be written as $\rho(x, t) = \rho(\omega, x) \exp(i\omega t)$. We consider the steady state under the action of external oscillating fields. See (Bazant *et al* 2004) for a discussion of the transient case. The spatial dependence of the density amplitude $\rho(\omega, x)$ can be taken to be proportional to $\sinh(qx)$. It can be checked by direct substitution that $\rho(\omega, x)$ satisfies Eq. (14) for suitable choice of the parameter q. Terms proportional to $\cosh(qx)$ must be set to zero to maintain electroneutrality. The parameter q must satisfy the dispersion relation:

$$i\omega = D[q^2 - \kappa^2]. \tag{17}$$

The parameter q can be interpreted as a complex inverse screening length. At low frequencies, $q \approx \pm \kappa [1 + i\omega/(2D\kappa^2)]$. From here on, the symbol q denotes the root with the positive value. In addition to the characteristic length κ^{-1} , the properties of the electrolyte determine a characteristic frequency $\Omega_{\rm E}$:

$$\Omega_{\rm E} = D\kappa^2 = \sigma_0/(\varepsilon_0 \varepsilon_{\rm E}). \tag{18}$$

Note that this characteristic frequency is associated with the electrolyte and not with the full system comprising a series of confined electrolytes. The characteristic frequency of the whole system can be orders of magnitude smaller. However, Ω_E serves as a reference to observe the emergence of the low-frequency behavior.

The charge density is concentrated in the double layers created at the walls confining the electrolyte region. We assume that the electrolyte region thickness $L_{\rm D}$ is several times larger than the screening length κ^{-1} . Away from the origin at the center of the electrolyte region, the density, proportional to $\sinh(qx)$, is dominated by the exponential terms $\exp(qx)$ for x>0 and $\exp(-qx)$ for x<0. Thus, near each of the wall boundaries at $x=\pm L_{\rm E}/2$, the density is given by an exponentially-decaying oscillatory function. The magnitude of the inverse decay length is of the order of the screening length $(q\sim\kappa)$. It is useful to express this density as a function of the distance away from the wall. Without any loss of generality, we consider the left end of the region located at $x=-L_{\rm E}/2$, and introduce a local variable $x'=x+L_{\rm E}/2$. The charge density is then well approximated by $\rho\approx P\exp[-q(x+L_{\rm E}/2)]=P\exp[-qx']$ (with P being a frequency dependent amplitude). Similarly, near the right wall at $x=L_{\rm E}/2$, $\rho=-P\exp[q(x-L_{\rm E}/2)]$.

The charge density generates a potential ϕ_c that must satisfy the Poisson equation, equation (15). Near the left boundary, the solution takes the form

$$\phi_c(\omega, x') = -[P/\varepsilon_0 \varepsilon_E q^2] \exp[-qx']. \tag{19}$$

This expression, along with its corresponding part at the right wall, provides the inhomogenous solution indicated in equation (16).

The electric field associated with the above inhomogeneous potential is $E_c = [P/\varepsilon_0 \varepsilon_E q] \exp[-qx']$ near the left wall. It creates an ionic current contribution $\sigma_0 E_c = (D\kappa^2/q)P \exp[-qx']$. The diffusion current is proportional to the gradient of the charge density $-D\nabla \rho = -DqP \exp[-qx']$. The amplitude of the net ionic current near the wall is then, using equations (11) and (16)

$$j(\omega, x') = \left(-\frac{\kappa^2}{q} + q\right) DP \exp(-qx') + \sigma_0 E_{\rm B}.$$
 (20)

This quantity must equal zero at the left wall, i.e. $j(\omega, 0) = 0$. Solving this relation for the charge density amplitude P and using equation (17) leads to:

$$P = \frac{iq\sigma_0}{\omega} E_{\rm B}.$$
 (21)

This relation can also be obtained via a time-integration of the current density across the midpoint of the region, which is just proportional to E_B . The above derivation highlights the use of the hard-wall condition.

Equation (21) yields the charge density $\rho = (iq\sigma_0 E_B/\omega) \exp[-qx']$, which determines the amplitude of the potential ϕ_c created by the charges near the confining wall. As the charge density decays quickly into the bulk, a net total charge per unit area Q at the wall can be obtained by integration over the double layer region:

$$Q = \frac{i\sigma_0}{\omega} E_{\rm B}.$$
 (22)

This total charge amplitude characterizes the dynamic double layer. It is clearly out-of-phase with respect to the bulk field. The electric field at both walls is the same by symmetry, and has the value $E_{\rm S} = -\nabla \phi_c(\omega, \pm L_{\rm E}/2) + E_{\rm B}$, which can be written in terms of the bulk field $E_{\rm B}$ as

$$E_{\rm S} = -i\frac{Dq^2}{\omega}E_{\rm B}.$$
 (23)

The potential difference across the electrolyte region due to accumulated charges near the dielectric walls can also be expressed in terms of the bulk field as $2i(D\kappa^2/q\omega)E_B$. The total potential difference in the electrolyteregion $\Delta\Phi_S(\omega)$ is the sum of this term and the one due to the bulk field, which is $-E_BL_E$ from equation (16):

$$\Delta\Phi_{S}(\omega) = \left[-L_{E} + i\frac{2D\kappa^{2}}{q\omega}\right]E_{B}.$$
(24)

Finally we note that in our 1D model system, symmetry dictates that there is no accumulated charge at the center (x = 0) of the electrolyte region. However, the x-component of the electromagnetic current at x = 0, $J(\omega)$, is finite and takes the value

$$J(\omega) = \sigma_0 E_{\rm B} + i\omega \varepsilon_E \varepsilon_0 E_{\rm B} = \varepsilon_E \varepsilon_0 D q^2 E_{\rm B}, \tag{25}$$

where the second equality follows from the dispersion relation in equation (17).

3.2. Dielectric wall

We consider the dielectric wall region centered at x=-L/2 of width $L_{\rm D}$ confining the electrolyteregion considered above centered at x=0. Below, we only show the non-trivial, x-component of the vectors associated with the 1D model. Within the dielectric wall characterized by a relative permittivity $\varepsilon_{\rm D}$, there are no unbound charges and the electric field is spatially uniform:

$$E(x, t) = E_{\rm D} \exp[i\omega t], \tag{26}$$

where, E_D is the amplitude in the frequency domain. E_D can be determined via the continuity condition of the displacement field at the boundary between the dielectric wall and the electrolyte solution:

$$\varepsilon_{\rm D}E_{\rm D}=\varepsilon_{\rm E}E_{\rm S},$$
 (27)

where E_S is the electric field at the edge within the electrolyteregion. Substituting E_S from equation (23) yields

$$E_{\rm D} = -i \frac{\varepsilon_{\rm E}}{\varepsilon_{\rm D}} \frac{Dq^2}{\omega} E_{\rm B}. \tag{28}$$

The total potential difference across the dielectric wall region is simply $\Delta\Phi_{\rm D}=-L_{\rm D}E_{\rm D}$, which yields

$$\Delta\Phi_{\rm D} = i \frac{\varepsilon_{\rm E}}{\varepsilon_{\rm D}} \frac{L_{\rm D} D q^2}{\omega} E_{\rm B}.$$
 (29)

Finally, the ionic current in the dielectric wall region vanishes, $j(\omega, x) = 0$. However, there is an electromagnetic current within this region which is equal to the displacement current $J(\omega) = j_D(\omega, x) = i\omega\varepsilon_0\varepsilon_D E_D = \varepsilon_E\varepsilon_0 Dq^2 E_B$. The last equality and equation (25) demonstrate the conservation of the electromagnetic current.

3.3. Impedance and conductivity

The impedance of a material is a directly measurable quantity and is calculated by obtaining the potential drop (the negative of the potential difference) necessary to create a given electromagnetic current. In a region of length

L consisting of an electrolyte solution of length $L_{\rm E}$ and a dielectric wall of thickness $L_{\rm D}$, the drop is $V(\omega) = -\Delta\Phi_{\rm S} - \Delta\Phi_{\rm D}$. Following equations (24) and (29), we obtain

$$V(\omega) = \left(L_{\rm E} - i\frac{2D\kappa^2}{q\omega} - i\frac{\varepsilon_{\rm E}}{\varepsilon_{\rm D}}\frac{L_{\rm D}Dq^2}{\omega}\right)E_{\rm B}.$$
 (30)

Using the relation between the electromagnetic current $J(\omega)$ and E_B in equation (25), we find

$$V(\omega) = \frac{L}{\varepsilon_{\rm E} \varepsilon_0 D q^2} \left(\ell_{\rm E} - i \frac{2D\kappa^2}{q\omega L} - i \frac{\varepsilon_{\rm E} \ell_{\rm D} D q^2}{\varepsilon_{\rm D} \omega} \right) J(\omega), \tag{31}$$

where we have recalled the length ratios: $\ell_E = L_E/L$ and $\ell_D = L_D/L$. The impedance Z of the repeating unit of size L of transverse area A is

$$Z = \frac{V(\omega)}{AJ(\omega)} = \frac{L}{A\varepsilon_{\rm E}\varepsilon_0 Dq^2} \left(\ell_{\rm E} - i \frac{2D\kappa^2}{q\omega L} - i \frac{\varepsilon_{\rm E}\ell_{\rm D} Dq^2}{\varepsilon_{\rm D}\omega} \right),\tag{32}$$

where the last equality easily follows from equation (31).

The impedance of the composite structure comprising N repeats of the unit structure is NZ. The conductivity is defined as the inverse of the impedance per unit length divided by the transverse area, $\sigma(\omega) = (NL/NZ)/A = L/(ZA)$. This is also consistent with the macroscopic relation in equation (7), $\sigma(\omega) = E_{av}/J(\omega)$, since $E_{av} = V/L$. Using equation (32), we obtain

$$\sigma(\omega) = \frac{\omega(q^2/\kappa^2)\sigma_0}{\ell_E \omega - i \left(\frac{\varepsilon_E \ell_D}{\varepsilon_D} D q^2 + \frac{2}{qL} D \kappa^2\right)},$$
(33)

where we have used the second equality in equation (18) to introduce the intrinsic conductivity σ_0 for a monovalent electrolyte. In obtaining this result we have used multiple repeats of an assumed periodic unit. If the repeat units are not identical, the impedance is a sum of terms shown in equation (32). Each contribution depends on the local dimensionless parameters ℓ_D , ℓ_E and κL . The impedance as well as the effective conductivity are averages over these contributions and thus determined by the average values of these parameters.

Equation (33) is the key result of this paper. We now present this result in a simplified form by introducing a characteristic frequency parameter Ω :

$$\Omega(\omega) = D\kappa^2 \left(\frac{\ell_D \varepsilon_E}{\ell_E \varepsilon_D} \frac{q^2}{\kappa^2} + \frac{2}{qL} \frac{1}{\ell_E} \right)$$
 (34)

and a characteristic scale $\sigma^{\rm E}$ for the conductivity:

$$\sigma^{E}(\omega) = \frac{\sigma_0}{\ell_{E}} \left(1 + i \frac{\omega}{\Omega_{E}} \right), \tag{35}$$

where $\Omega_E = D\kappa^2$ is the characteristic frequency associated with the pure electrolyte, given in equation (18). With these definitions, the conductivity becomes:

$$\sigma(\omega) = \frac{\omega}{\omega - i\Omega} \sigma^{E}.$$
 (36)

Equation (36) has a structure similar to a Debye conductivity form (see below), with a key difference: both Ω and σ^E are frequency-dependent and complex; in the case of the former, this becomes evident by noting that q is complex and frequency dependent as seen in equation (17).

In the limiting case of $\omega \to 0$, both σ^E and Ω have real limits: σ_0^E and Ω_0 , respectively: $\sigma_0^E = \sigma_0/\ell_E$ is the conductivity associated with the electrolyteregion, while Ω_0 is given by

$$\Omega_0 = \Omega_{\rm E} \left(\frac{\ell_{\rm D} \varepsilon_{\rm E}}{\ell_{\rm E} \varepsilon_{\rm D}} + \frac{2}{\kappa L} \frac{1}{\ell_{\rm E}} \right). \tag{37}$$

Here we have used $\Omega_E = D\kappa^2$ and the fact that $q \approx \kappa$ for $\omega \to 0$. Ω_0 represents the characteristic frequency of the composite system characterized by electrolyte and dielectric wall regions, and can be interpreted as the inverse of the characteristic relaxation time associated with the double layer buildup process. As evident by the ratio Ω_0/Ω_E :

$$\frac{\Omega_0}{\Omega_E} = \frac{\varepsilon_E}{\varepsilon_D} \frac{\ell_D}{\ell_E} + \frac{2}{\kappa L} \frac{1}{\ell_E},\tag{38}$$

 Ω_0 can be orders of magnitude smaller than the characteristic frequency Ω_E associated with the pure electrolyte, for example, under high electrolyte concentration such that $\kappa L \gg 1$ and when $\ell_E \gg \ell_D$.

Using σ_0^E and Ω_0 in equation (33), the low-frequency limit for the conductivity becomes:

$$\sigma(\omega) \approx \frac{\omega}{\omega - i\Omega_0} \sigma_0^{\rm E},\tag{39}$$

which seamlessly retrieves the standard Debye form. The complex conductivity can be written as $\sigma = \sigma' + i\sigma''$ where σ' and σ'' are its real and imaginary parts. At low frequencies these take the form

$$\sigma'(\omega) \approx \frac{\omega^2}{\omega^2 + \Omega_0^2} \frac{\sigma_0}{\ell_E} \left(1 - \frac{\Omega_0}{\Omega_E} \right), \tag{40}$$

$$\sigma''(\omega) \approx \frac{\omega \Omega_0}{\omega^2 + \Omega_0^2} \frac{\sigma_0}{\ell_E}.$$
 (41)

The complex, frequency-dependent relative permittivity $\varepsilon(\omega)$ is given by $\varepsilon(\omega) = \varepsilon'(\omega) + i\varepsilon''(\omega) = (\sigma'' + i\sigma')/(\varepsilon_0\omega)$. In the low frequency limit, the real and imaginary parts of $\varepsilon(\omega)$ are

$$\varepsilon'(\omega) \approx \frac{\Omega_0}{\omega^2 + \Omega_0^2} \frac{\sigma_0}{\varepsilon_0 \ell_{\rm E}},$$
 (42)

$$\varepsilon''(\omega) \approx \frac{\omega}{\omega^2 + \Omega_0^2} \frac{\sigma_0}{\varepsilon_0 \ell_E} \left(1 - \frac{\Omega_0}{\Omega_E} \right). \tag{43}$$

The real part of the permittivity has the zero frequency limit

$$\varepsilon'(\omega \to 0) = \frac{\sigma_0}{\varepsilon_0 \ell_E \Omega_0} = \frac{\varepsilon_E}{\ell_E} \left(\frac{\ell_D \varepsilon_E}{\ell_E \varepsilon_D} + \frac{2}{\kappa L} \frac{1}{\ell_E} \right)^{-1}. \tag{44}$$

As discussed below, this expression produces large numerical values for permittivity that match with the experimental values. The imaginary part of the permittivity goes to zero as $\omega \to 0$.

In addition to recovering the Debye-type forms for conductivity at low frequencies, the general result for conductivity in equation (33) has a clear interpretation at high frequencies. The high-frequency limit gives

$$\lim_{\omega \to \infty} \sigma(\omega) = i \frac{\sigma_0 \omega}{\Omega_E} \frac{\varepsilon_D}{\varepsilon_D \ell_E + \varepsilon_E \ell_D} = \frac{i \omega \varepsilon_0}{\ell_E / \varepsilon_E + \ell_D / \varepsilon_D}.$$
 (45)

Using this expression, we find that the high frequency limit for relative permittivity $\varepsilon(\omega)$ is real:

$$\lim_{\omega \to \infty} \varepsilon(\omega) = \frac{1}{\ell_{\rm E}/\varepsilon_{\rm E} + \ell_{\rm D}/\varepsilon_{\rm D}},\tag{46}$$

and can be expressed as a weighted harmonic mean of the permittivities associated with the electrolyte and dielectric wall regions (noting that $\ell_E + \ell_D = 1$). In the limiting case of the pure electrolyte, $\ell_E \to 1$ (and $\ell_D \to 0$), we recover $\lim_{\omega \to \infty} \varepsilon(\omega) = \varepsilon_E$. Similarly, in the case of a very thin electrolyteregion characterized by $\ell_E \to 0$ (and $\ell_D \to 1$), we obtain $\lim_{\omega \to \infty} \varepsilon(\omega) = \varepsilon_D$.

4. Results

4.1. Examples

We begin by showing results for a system composed of repeated electrolyteregions of characteristic length $L_{\rm E}=19\kappa^{-1}$ separated by dielectric walls of thickness $L_{\rm D}=\kappa^{-1}$. The total length of the repeated unit associated with the composite system is $L=20\kappa^{-1}$. The electrolyte solvent is assumed to be water, with permittivity $\varepsilon_{\rm E}=80$, while the dielectric region has permittivity $\varepsilon_{\rm D}=20$. With these values, the characteristic real frequency of the composite system follows from equation (37) as $\Omega_0=0.2~\Omega_{\rm E}$, where $\Omega_{\rm E}$ is the characteristic frequency of the pure electrolyte. The parameters characterizing this example system are selected to clearly illustrate the long-range structural features of the associated fields and currents in order to highlight the influence of the heterogeneous material structure on the electrical properties of the model system.

Figure 3 shows the structure of the electric potential, the electric field, ionic current, displacement current, and the charge density associated with this example system when an external oscillating electric field of frequency $\omega=0.095~\Omega_{\rm E}$ is applied. The plots show the real and imaginary amplitudes of these quantities as a function of position x, which is measured in units of the screening length κ^{-1} . The real part of these amplitudes, the in-phase component, can be considered as snapshots obtained when the external field is maximum. The imaginary parts correspond to times when the external field is zero and increasing. The potential, field, current, and charge density are measured in units of Φ_U , E_U , j_U , and ρ_U , respectively. The reference potential and field values are $\phi_U=e\kappa/\varepsilon_0\varepsilon_E$ and $E_U=e\kappa\Phi_U=e\kappa^2/\varepsilon_0\varepsilon_E$ respectively. The current is expressed in multiples of $j_U=\sigma_0E_U=e\kappa^2\Omega_c$, and the charge density is expressed in multiples of $\rho_U=e\kappa^3$. In these units, the average value of the magnitude of the external electric field used is 1 unit.

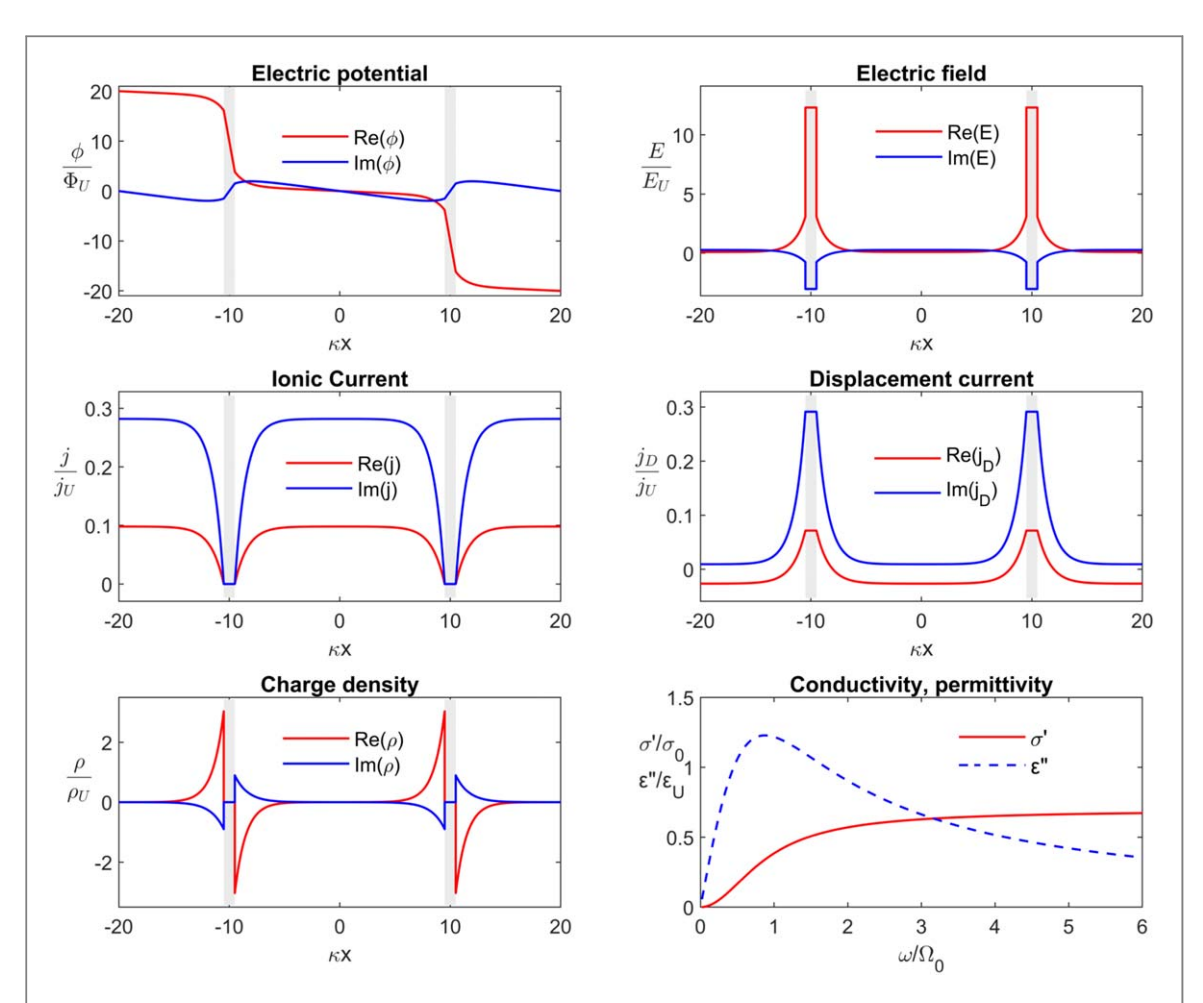


Figure 3. Electrical properties (potential ϕ , field E, ionic current j, displacement current j_D, and charge density ρ) of a heterogeneous system characterized with alternating sequence of electrolyteregions of length $19\kappa^{-1}$ and dielectric walls (shaded gray) of thickness κ^{-1} . The characteristic frequency is $\Omega_0=0.2~\Omega_{\rm E}$. Results are shown as a function of the position x for an external oscillating electric field of frequency $\omega=0.095~\Omega_{\rm E}$. The bottom right subplot shows the variation in the real part of the conductivity and permittivity as ω is changed. See the main text for the meaning of other symbols and model system details.

In a homogeneous system (pure electrolyte), the potential amplitude would be real and its plot would simply be a line of slope -1. The situation is dramatically different for the heterogeneous composite system considered here, where the potential ϕ has non-zero real and imaginary parts, and exhibits nonlinear features. The real part is characterized with a sharp drop within the dielectric walls, where ϕ is linear. In the electrolyteregion, ϕ is approximately linear in the bulk but exhibits a nonlinear variation near the walls due to the presence of the dynamic double layers. The imaginary part of the potential is approximately zero, however, we observe a small non-vanishing amplitude localized near the walls.

The electric field exhibits a variation with position that is consistent with the negative gradient of the potential. The field is the negative of the gradient of the potential and is constant within the dielectric walls. It has a very small value in the bulk of the electrolyteregion. This nearly vanishing field produces a small and uniform ionic current in the bulk. The ionic current transitions, near the electrolyte boundaries to is zero value within the walls. The displacement current is largest and uniform within the walls, and exhibits a variation with position in the electrolyteregion that is consistent with the conservation of the full electromagnetic current. In the bulk of the electrolyteregion, the numerical value of the electromagnetic current is approximately the same as the ionic current. Finally, the charge density exhibits an the accumulation and depletion of ions at the opposite end the walls. These are the dynamic double layers. The charge density vanishes within the dielectric walls.

Figure 3 also shows the real part of the conductivity in units of the electrolyte conductivity σ_0 as a function of the frequency ω scaled by Ω_0 . The small ionic current in the bulk is responsible for the overall reduction of the real part of the renormalized conductivity observed at low ω . The corresponding imaginary part of the permittivity, scaled by the factor $\varepsilon_U = \varepsilon_E \Omega_E/\Omega_0 = 400.0$, as a function of ω is also shown. We observe a peak in the permittivity at a frequency ω near the characteristic real frequency Ω_0 of the heterogeneous system. The system thus shows a β -relaxation.

Systems characterized with $L_{\rm E}\gg L_{\rm D}$ (i.e. when the thickness of the electrolyteregion is much larger than the thickness of the wall) produce a much greater reduction of the characteristic real frequency Ω_0 of the composite

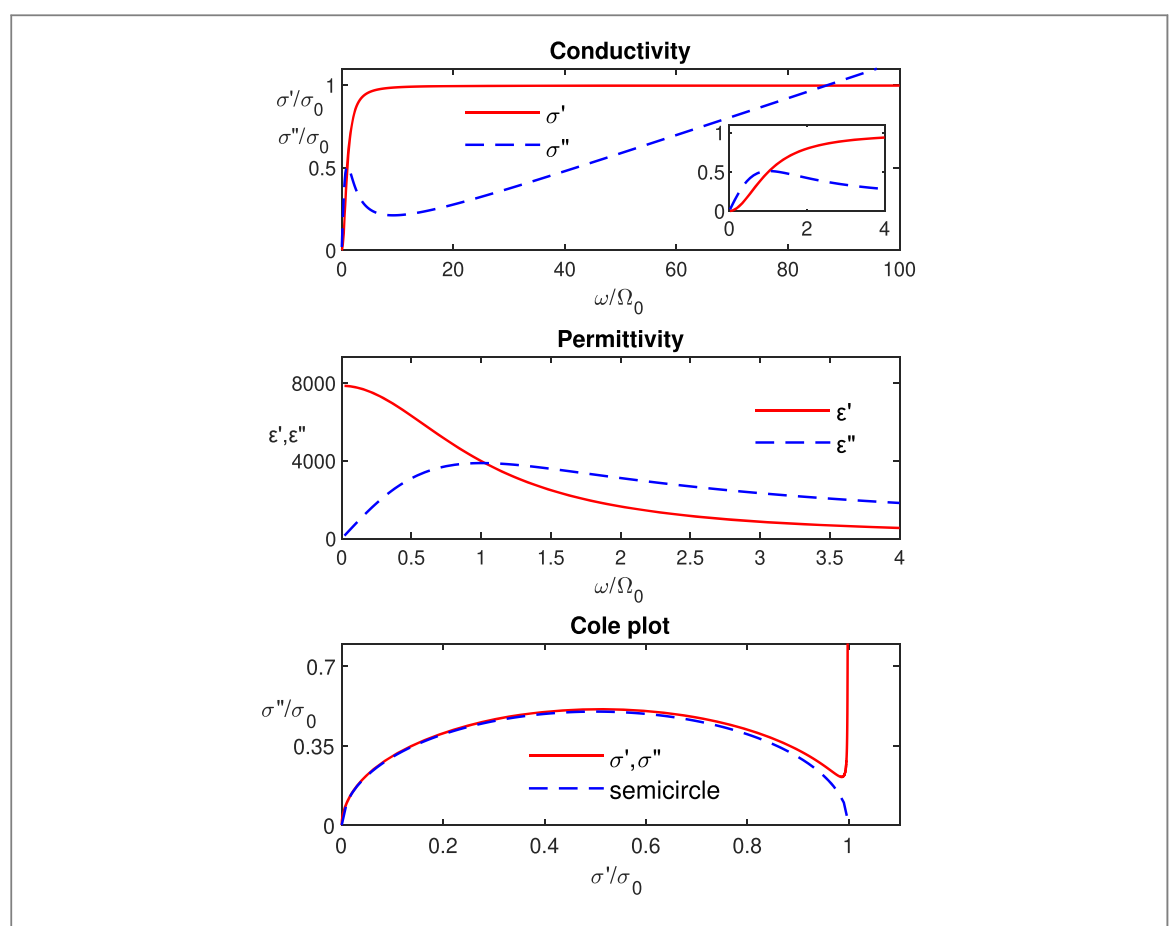


Figure 4. Electrical properties of a heterogeneous system characterized with alternating sequence of electrolyteregions of length $199\kappa^{-1}$ and dielectric walls of thickness κ^{-1} . Top panel shows the real and imaginary parts of the conductivity $\sigma = \sigma' + i\sigma''$ as a function of the frequency ω of the applied external electric field. Middle panel shows the variation of the real and imaginary parts of the permittivity $\varepsilon = \varepsilon' + i\varepsilon''$ with ω . The bottom panel shows the Cole plot showing the variation of σ'' against σ' . Electrical conductivity tracks the standard semicircular shape in the low-frequency regime. However, at high frequencies, the linear growth in σ'' leads to a vertical asymptote. See the main text for the meaning of other symbols and model system details.

structure with respect to that of the pure electrolyte Ω_E . For example, a composite system of total length $L=200\kappa^{-1}$ with $L_E=199\kappa^{-1}$ and $L_D=1\kappa^{-1}$ (such that $\ell_E/\ell_D=199$) leads to $\Omega_0=0.03~\Omega_E$, keeping all other model parameters the same as above. The top two panels in figure 4 show the complex conductivity (scaled by the intrinsic conductivity of the pure electrolyte σ_0) and the complex relative permittivity as a function of the frequency ω for this example system. The bottom panel shows the Cole plot with the imaginary part of the conductivity plotted against its real part. Both the real and imaginary parts of the normalized conductivity have a limiting value of zero as $\omega \to 0$. At large frequencies, the imaginary part of the normalized conductivity dominates over the real part, which rapidly saturates to $1/\ell_E \approx 1$, where we take $\ell_E \to 1$ and $\ell_D \to 0$ (given $\ell_E \gg \ell_D$). The imaginary part grows linearly with ω for large frequencies and taking $\ell_E \to 1$ and $\ell_D \to 0$ in equation (45), the slope of this linear growth is approximately ε_E . In a Cole plot, the linear growth leads to a vertical asymptote after the real and imaginary parts closely track the semicircle shape.

The imaginary part of the permittivity approaches zero value as $\omega \to 0$. However, taking $\ell_E \to 1$ and $\ell_D \to 0$ in equation (46), shows that the real part of the relative permittivity approaches $\epsilon_E \kappa L$ which is \approx 8000 for this example system with $\kappa L=200$ and $\varepsilon_E=80$. At low frequencies, a clear peak in the imaginary part of the permittivity is observed, indicating the presence of the β dispersion. As $\omega \to \infty$, the imaginary part of the permittivity tends to zero while the real part approaches $\varepsilon_E=80$.

4.2. Layered systems

To understand the effect of the dynamic double layers in determining the electrical properties of the confined electrolyte system, it is useful to contrast the above results with a simpler model where these details play no significant role. For very small screening lengths, one can consider a layered system of alternating piecewise-uniform slabs of materials of permittivity and conductivity with constant (frequency independent) real parts. These alternating slabs (k = 1, 2) have complex conductivities $\sigma^{(k)} = \sigma_{0k} + i\omega\varepsilon_0\varepsilon_k$ and lengths L_k . Their impedances per unit area have values $Z_k = L_k/(A\sigma^{(k)})$. A system of multiple repeated units of these slabs has an effective macroscopic conductivity $\sigma_Y = (L/A)(Z_1 + Z_2)^{-1}$, which is the weighted harmonic mean of the

Table 1. Parameters for selected vegetable tissues.

Sample	$L_{\rm E}(\mu{ m m})$	$L_{\rm D}({\rm nm})$	$\kappa^{-1}(\mathrm{nm})$	$\varepsilon_{ m E}$	$arepsilon_{ m D}$	$\sigma_0(\text{S m}^{-1})$	$\frac{1}{2\pi}\Omega_0(\text{MHz})$	$f_{\beta}(\text{MHz})$
Carrot	60	8.2	0.96	80	2.3	0.66	7.0	5.0
Banana	80	10.4	0.96	80	2.3	0.54	5.5	7.0
Potato	100	11.6	0.96	80	2.3	0.84	7.6	6.0

conductivities of the components:

$$\sigma_Y = \left(\frac{\ell_1}{\sigma^{(1)}} + \frac{\ell_2}{\sigma^{(2)}}\right)^{-1} = \frac{\sigma^{(1)}\sigma^{(2)}}{\ell_1\sigma^{(2)} + \ell_2\sigma^{(1)}},\tag{47}$$

where the relative lengths $\ell_k = L_k/L$ act as the weights.

The individual uniform slabs do not have a Debye-type conductivity, but the combined layered system does. This is evident by examining the denominator in the last equality in equation (47), which has the form $\ell_1 \sigma^{(2)} + \ell_2 \sigma^{(1)} = \ell_1 \sigma_{02} + \ell_2 \sigma_{01} + i\omega \varepsilon_0 (\ell_1 \varepsilon_2 + \ell_2 \varepsilon_1)$, similar to the expression in the denominator of equation (40). For the case of an electrolyte slab of thickness ratio $\ell_1 \equiv \ell_E$ and permittivity $\varepsilon_1 \equiv \varepsilon_E$ alternating with a dielectric slab of thickness ratio $\ell_2 \equiv \ell_D$ and permittivity $\varepsilon_2 \equiv \varepsilon_D$, the real part of the denominator term is $\ell_D \sigma_0$. Here, σ_0 is the real part of the conductivity of the pure electrolyte and we assume that the conductivity of the dielectric slab is much smaller. The imaginary part has the form $i\omega \varepsilon_0 \bar{\varepsilon}$ with mean permittivity $\bar{\varepsilon} = \ell_D \varepsilon_E + \ell_E \varepsilon_D$. Considering the electrolyte region to be much longer than the dielectric slab, we get $\bar{\varepsilon} \approx \ell_E \varepsilon_D$ and the imaginary part becomes $i\omega \varepsilon_0 \ell_E \varepsilon_D$. This layered system exhibits a characteristic frequency

$$\Omega_{Y} = \frac{\ell_{D}\sigma_{0}}{\varepsilon_{0}\ell_{E}\varepsilon_{D}} = \frac{\ell_{D}\varepsilon_{E}}{\ell_{E}\varepsilon_{D}}\Omega_{E}.$$
(48)

This direct calculation matches the low-frequency $(\omega \to 0)$ limiting value of the characteristic frequency Ω , in equation (34), associated with the microscopic model of the heterogeneous confined electrolyte system when $(\kappa L)^{-1} \ll \ell_D \varepsilon_E / (\ell_E \varepsilon_D)$.

In both the layered system and the microscopic model, the typically small value of the ratio ℓ_D/ℓ_E suppresses the associated characteristic frequency $(\Omega_Y \text{ or } \Omega)$ to values much smaller than the characteristic frequency Ω_E of the fully uniform and homogeneous pure electrolyte system. Control of this ratio is the key to generating the characteristic values for the α and β dispersion regimes. The layer geometry can serve as the basis to introduce more complex modeling of specific systems. In particular, we note that the assumption of a purely dielectric wall can be relaxed to include the presence of mobile ions in the extracellular region, providing a small effective conductivity to the model layer representing it.

4.3. Interpreting experimental measurements

Our model with dynamic double layers and even the simplified multiple slab systems produce good quantitative results in concrete systems. For example, vegetable tissues have been well characterized by means of impedance spectroscopy. Properties such as typical cell sizes can also be directly determined in the same samples by optical microscopy. Reported conductivity measurements for banana, carrot and potato show clear β dispersion behavior. From published data (Angersbach *et al* 1999), a characteristic frequency f_{β} (in MHz) can be obtained from the mid-points of the transition between plateaus of the (real) conductivity. The model discussed above can broadly match the location of this frequency to the characteristic value Ω_0 or Ω_Y . To this end, we use values of the relevant parameters (L_D , L_E , σ_0 , ε_E , ε_D) that have been measured or estimated for these three samples (Angersbach *et al* 1999), as noted in table 1.

In these example systems, the electrolyte region is identified with the cytosol and vacuole of the cells, which span most of the volume of the cells. We take the cell linear size as $L_{\rm E}$ and use the water permittivity to characterize the permittivity $\varepsilon_{\rm E}=80$ in this region. The thickness of the dielectric region $L_{\rm D}$ is identified with twice the cell membrane thickness and the permittivity of this region is taken to be $\varepsilon_{\rm D}=2.3$. The inverse screening length is estimated to be $\kappa\approx0.96$ nm $^{-1}$, which corresponds to cytosolic ionic strength of 100 mM. We note that the dimensionless factor $(\kappa L_{\rm E})^{-1}$ is very small so that both estimates of characteristic frequencies effectively coincide $\Omega_0\approx\Omega_Y$.

The estimated values used for the electrolyte conductivity, $\sigma_0 \approx 0.7~\mathrm{S~m}^{-1}$ can be compared with direct calculations based on typical properties of cells. Interpreting the physiological ionic strength of 100 mM as associated with just monovalent ions, and using the average of mobility values for sodium and chloride ions $(5.2 \times 10^{-8} \,\mathrm{and}\, 7.7 \times 10^{-8} \,\mathrm{m}^2 \,\mathrm{(V~s)}^{-1}$ respectively (Atkins and De Paula 2011)), one obtains an electrolyte conductivity $\sigma_0 = 1.24~\mathrm{S~m}^{-1}$. This value is large compared to the one noted in table 1. This suggests a reduced effective mobility for ions in cells, which is expected as some of these ions can be bound to organelles or cell

membranes and thus not directly participate in conductive motion. This analysis is a simplified version of that presented by Angersbach et al (Angersbach et al 1999), which uses many more parameters. As noted, the correction due to the dynamic double layers is in fact small. However, the explicit expressions obtained by the microscopic model allow evaluation of quantities characterizing the internal structure of these systems. Equation (45) shows that at high frequency, the conductivity result is not simply σ_0 . The conductivity is in fact dominated by its imaginary part which grows linearly with frequency at high frequency. The behavior of high-frequency permittivity, which is purely real, provides a clearer comparison with experiments. Following equation (46), permittivity at high frequencies is $\epsilon(\omega) \approx \varepsilon_E \varepsilon_D / (\varepsilon_D \ell_E + \varepsilon_E \ell_D)$, which is dominated by the permittivity in the electrolyte region when the latter's thickness is much larger than the thickness of the dielectric wall (i.e. when $\ell_E \approx 1$, $\ell_D \approx 1$). Values of high-frequency permittivity close to those of water (\approx 80) have been recorded in all published data of watertissue (Gabriel et al 1996b, Angersbach et al 1999, Gabriel et al 2009).

Next we examine the behavior of permittivity at low frequencies, for which we have obtained a limiting value in equation (44). In the case of $\ell_E \approx 1$, and very small screening lengths $(\kappa L)^{-1} \ll \ell_D \varepsilon_E / (\ell_E \varepsilon_D)$, this limiting value becomes $\epsilon'(\omega \to 0)^- \varepsilon_D / \ell_D$. In other words, it is the ratio of relative permittivity and relative thickness of the dielectric wall region. Using the aforementioned values for vegetable tissues ($\varepsilon_D = 2$, $\ell_D = 1.25 \times 10^{-4}$), one obtains $\varepsilon(\omega \to 0) \sim O(10^4)$, which matches experimental permittivity values recorded for most vegetable and animal tissues (Gabriel *et al* 1996b, Angersbach *et al* 1999, Gabriel *et al* 2009).

The expression for the low-frequency permittivity in the limiting case of $\ell_{\rm E}\approx 1$ and small screening lengths can also be recovered from the model of a layered system, without appeal to the internal structure of the material. Following a similar calculation as above for the case of an electrolyteslab of thickness ratio $\ell_1 \equiv \ell_{\rm E}$, permittivity $\varepsilon_1 \equiv \varepsilon_{\rm E}$, and conductivity $\sigma_{01} \equiv \sigma_0$ alternating with a dielectric slab of thickness ratio $\ell_2 \equiv \ell_{\rm D}$, permittivity $\varepsilon_2 \equiv \varepsilon_{\rm D}$, and conductivity $\sigma_{02} \approx 0$, the imaginary part of the conductivity in the limit of $\omega \to 0$ becomes $\omega \varepsilon_0 \varepsilon_{\rm D}/\ell_{\rm D}$. This immediately yields $\varepsilon'(0) = \varepsilon_{\rm D}/\ell_{\rm D} = \varepsilon_{\rm D} L/L_{\rm D}$, where the first equality is exactly the result derived above using the microscopic model, and the second equality just expands the definition of the thickness ratio.

We find that the zero-frequency limit of the permittivity is essentially the permittivity of the dielectric layer multiplied by a geometric factor $L/L_{\rm D}=1/\ell_{\rm D}$ that compares the total size of the repeated unit to the thickness of the dielectric region. This observation can be used to discuss the appearance of very large relative permittivities. In most tissues the values are large, in the 10^5 range. However, in some cases these values can reach 10^7 (heart tissue, for example (Gabriel *et al* 1996b, 1996)). Our results show that such permittivities require the size ratio $\ell_{\rm D}^-1$ to be very large. A way to obtain this large ratio is to consider the presence of strong heterogeneities where dielectric regions are separated by very large, more conductive, regions. This scenario can arise when we consider systems where the extracellular matrix of a tissue plays the role of conductive regions. The bounding walls in this case are provided by ion-impermeable or low-conductivity tissues separating large multi-cellular regions. These large size ratios also depress the ratio of the value of the characteristic frequency to the electrolyte value $\Omega_0/\Omega_{\rm E}$. Therefore, systems that exhibit these features might also present permittivity peaks in the α -regime.

5. Discussion and conclusion

The above results show that the correction to the composite system due to the presence of the dynamic double layers is small. However, consideration of these features enables a clearer interpretation of several aspects of these systems, such as the origin of the large effective permittivities in experimental measurements. The confined electrolytes model developed above also enables a microscopic description of important tissue-related macroscopic phenomena such as the Maxwell-Wagner effect, which is the appearance of accumulated charges at the interfaces between regions of different conductivities. While at the microscopic level this is just the creation of the dynamic double layers (Takashima et al 1989), conductivity variations at the macroscopic level must also create charge accumulation. The effect has been noted for models with heterogenous regions such as those used for EEG analysis (Solis and Papandreou-Suppappola 2019) and in discussions of skin conduction (Bârlea et al 2008) and tissue characterization (Guermazi et al 2014). As a macroscopic effect, it is likely to appear as part of very low frequency behavior and thus will be connected with α dispersion processes (Grimnes and Martinsen 2010). As figure 3 shows, the charge density in a system with multiple compartments has large local variations. These variations can be spatially averaged to define a macroscopic charge density which is effectively zero in a macroscopically-homogeneous region. However, at the interface between distinct macroscopic regions, the average need not be zero. In a 1D case, the electromagnetic current is spatially constant but the associated average electric field in each of the different regions may not have the same value. Gauss' law then requires the presence of charge at the interface between regions. This macroscopic effect can be described using the microscopic model developed in this work.

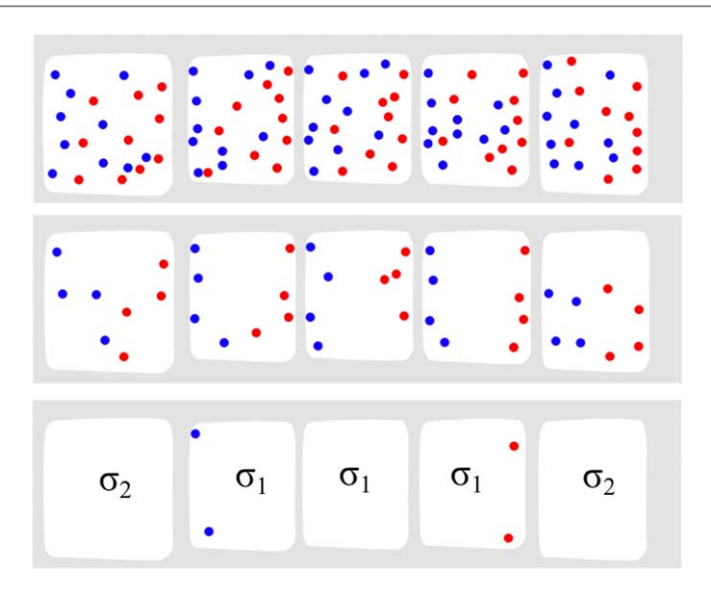


Figure 5. Within an AC cycle, the ions in the electrolyteregions accumulate at the dielectric walls, as shown in the top panel. The middle panel shows only the excess charge associated with the double layers. In the bottom panel, the neighboring double layers of regions with similar properties can be considered to cancel each other when averaged over large lengthscales. However, walls separating regions of different intrinsic properties acquire a net charge due to the differences in the interfacial charge distributions on either sides of the dielectric wall, leading to the emergence of the macroscopic Maxwell–Wagner effect.

A sketch of this scenario is shown in figure 5. The central part is composed of similar electrolyteregions, which are bounded by a couple of electrolyteregions with different intrinsic properties (e.g. different electrolyte concentrations). In the presence of an oscillatory field, the dynamic double layers appear at opposite sides of all dielectric walls. At walls between neighboring similar electrolytes, the accumulated charges are equal in magnitude and do not contribute to a macroscopic average. At walls separating regions with different properties, the double layers do not hold identical charge, which produces a macroscopically observable charge density. This construction is essentially the same as the elementary picture for the appearance of boundary charges in homogeneous polarizable materials. Namely, internal dipoles cancel macroscopically but those at boundaries contribute to net surface charges.

The macroscopic charge density that appears between regions of different properties can be calculated as follows. The conservation of electromagnetic currents in a 1D system can be expressed as

$$I^{(a)} = \sigma^{(a)}(\omega)E^{(a)} = \sigma^{(b)}(\omega)E^{(b)} = I^{(b)},\tag{49}$$

where $\sigma^{(k)}$ are the macroscopic average values of conductivities of the i^{th} electrolyteregion (where k=a,b), and $E^{(k)}$ and $J^{(k)}$ refer to the associated macroscopic electric fields and currents. The equality of the currents yields

$$\sigma^{(b)}(\omega)E^{(b)} - \sigma^{(a)}(\omega)E^{(a)} = \Delta\sigma E_{av} + \overline{\sigma}\Delta E = 0, \tag{50}$$

where $\Delta \sigma = \sigma^{(b)} - \sigma^{(a)}$ and $\overline{\sigma}$ are, respectively, the difference and mean value of conductivities. $E_{\rm av}$ is the average field that is uniform within each region in the 1D case, and ΔE is the jump in the electric field at the interface. By Gauss' law, the discontinuity in the electric field corresponds to a Maxwell–Wagner accumulated charge density $Q_{\rm MW} = \Delta E/\varepsilon_0$ at the interface. Following equation (50), we have the result

$$Q_{\rm MW} = -\frac{\Delta\sigma}{\overline{\sigma}} \frac{E_{\rm av}}{\varepsilon_0},\tag{51}$$

which indicates that an interface is electrified by the presence of a non-vanishing field. This relation remains macroscopically valid in the full three-dimensional case when the value $E_{\rm av}$ is identified as the field at the interface. The charge density $Q_{\rm MW}$ is a net charge that includes both ionic and polarization contributions, and thus there are many ways in which this net charge can appear. The scheme of figure 5, emphasizes the ionic component of the charge accumulation.

The model developed has important implications for low-frequency phenomena. In models for interpretation of electroencephalographic recordings and other biosignals, currents are considered quasi-stationary when the frequencies involved are below 10^3 Hz. These currents are assumed to satisfy continuity and constitutive equations with real constant conductivity in homogeneous regions (Geselowitz 1967, Mosher *et al* 1999, Nunez *et al* 2006). Discussion of these models can be carried out directly in terms of observed potentials, but the models intrinsically involve the Maxwell–Wagner effect and imply accumulation of charge at interfaces (Solis and Papandreou-Suppappola 2019). As discussed in section 2, the continuity is satisfied only for the electromagnetic current and not

its ionic component. Furthermore, at low frequencies the complex conductivity is mostly imaginary and thus has a capacitive rather than conductive nature. It is therefore crucial to reconsider these models to incorporate the complex form of the conductivity, which is not simply a minor correction.

The ideas developed here provide insight into several aspects of tissue conductivity. The key results predict specific functional forms for the conductivity that clearly show the presence of characteristic frequencies and provide correct limiting behaviors at low and large frequencies. Explicit consideration of the electrolyte behavior enables clear microscopic interpretations of currents, low-frequency polarization, and the Maxwell–Wagner effect. The proper consideration of the nature of currents informs the design of reliable models of macroscopic tissue behavior. The results can be extended to other geometries and can help design models for heterogeneous systems that explicitly use complex conductivities. Future work will also address the effects associated with the distribution of sizes of the wall-bounded electrolyte regions within the periodic structure employed in this work.

Acknowledgments

VJ was partially supported by National Science Foundation through Grant No. DMR-1753182.

Data availability statement

All data that support the findings of this study are included within the article.

ORCID iDs

Francisco J Solis https://orcid.org/0000-0002-3965-8024 Vikram Jadhao https://orcid.org/0000-0002-8034-2654

References

Abdalla S 2011 Low frequency dielectric properties of human blood IEEE Trans. Nanobiosci. 10 113–20

Åberg P, Birgersson U, Elsner P, Mohr P and Ollmar S 2011 Electrical impedance spectroscopy and the diagnostic accuracy for malignant melanoma Exp. Dermatol. 20 648–52

Angersbach A, Heinz V and Knorr D 1999 Electrophysiological model of intact and processed plant tissues: cell disintegration criteria *Biotechnol. Progr.* 15 753–62

Atkins P and De Paula J 2011 Physical Chemistry for the Life Sciences (Oxford: Oxford University Press)

Barbero G and Alexe-Ionescu A L 2005 Role of the diffuse layer of the ionic charge on the impedance spectroscopy of a cell of liquid *Liq. Cryst.* 32 943–9 Bârlea N, BÂrlea S I and Culea E 2008 Maxwell–Wagner effect on the human skin *Rom. J. Biophys.* 18 87–98

Bazant M Z, Thornton K and Ajdari A 2004 Diffuse-charge dynamics in electrochemical systems Phys. Rev. E 70 021506

Bouchaala D, Nouri H, Atitallah B B, Derbel N and Kanoun O 2021 Potential of impedance spectroscopy as a manifold non-invasive method for medical applications *Advanced Systems for Biomedical Applications* (Berlin: Springer) pp 1–23

Braun R P, Mangana J, Goldinger S, French L, Dummer R and Marghoob A A 2017 Electrical impedance spectroscopy in skin cancer diagnosis *Dermatol. Clin.* **35** 489–93

Brosseau C 2006 Modelling and simulation of dielectric heterostructures: a physical survey from an historical perspective *J. Phys. D: Appl. Phys.* 39 1277–94

Buck R P 1969 Diffuse layer charge relaxation at the ideally polarized electrode *J. Electroanal. Chem. Interfacial Electrochem.* 23 219–40 Cirkel P, Van der Ploeg J and Koper G 1997 Electrode effects in dielectric spectroscopy of colloidal suspensions *Physica* A 235 269–78 Crowell L L, Yakisich J S, Aufderheide B and Adams T N G 2020 Electrical impedance spectroscopy for monitoring chemoresistance of cancer cells *Micromachines* 11 832

Dukhin A S, Shilov V and Borkovskaya Y 1999 Dynamic electrophoretic mobility in concentrated dispersed systems. cell model *Langmuir* 15 3452–7

Dukhin S S, Shilov V N and Bikerman J J 1974 Dielectric phenomena and double layer in disperse systems and polyelectrolytes *J. Electrochem. Soc.* 121 154C

Eisenberg B 2018 Asking biological questions of physical systems: the device approach to emergent properties *J. Mol. Liq.* 270 212–7 Eisenberg B, Oriols X and Ferry D 2017 Dynamics of current, charge and mass *Comput. Math. Biophys.* 5 78–115

Eleiwa M A and Elsherbeni A Z 2001 Debye constants for biological tissues from 30 hz to 20 ghz Appl. Comput. Electromagn. Soc. J. 16 202–13 Fano R M, Adler R B and Chu L J 1963 Electromagnetic Fields, Energy, and Forces (London: Taylor and Francis)

Faucher S J et al 2019 Critical knowledge gaps in mass transport through single-digit nanopores: a review and perspective J. Phys. Chem. C 123 21309–26

Flores-Cosío G, Herrera-López E J, Arellano-Plaza M, Gschaedler-Mathis A, Kirchmayr M and Amaya-Delgado L 2020 Application of dielectric spectroscopy to unravel the physiological state of microorganisms: Current state, prospects and limits *Appl. Microbiol. Biotechnol.* 104 6101–13
Foster K R *et al* 1986 Dielectric properties of tissues *CRC Handbook of Biological Effects of Electromagnetic Fields* (Boca Raton, FL: CRC Press) pp 27–96

Fuller B D and Ward S H 1970 Linear system description of the electrical parameters of rocks *IEEE Trans. Geosci. Electron.* **8** 7–18 Gabriel C, Gabriel S and Corthout y E 1996 The dielectric properties of biological tissues: I. Literature survey *Phys. Med. Biol.* **41** 2231 Gabriel C, Peyman A and Grant E H 2009 Electrical conductivity of tissue at frequencies below 1 mhz *Phys. Med. Biol.* **54** 4863 Gabriel S, Lau R W and Gabriel C 1996a The dielectric properties of biological tissues: II. Measurements in the frequency range 10 hz to 20 ghz *Phys. Med. Biol.* **41** 2251

Gabriel S, Lau R W and Gabriel C 1996b The dielectric properties of biological tissues: III. Parametric models for the dielectric spectrum of tissues *Phys. Med. Biol.* 41 2271

Geselowitz D B 1967 On bioelectric potentials in an inhomogeneous volume conductor Biophys. J. 7 498-507

Grech R et al 2008 Review on solving the inverse problem in EEG source analysis J. Neuroeng. Rehabil. 5 33

Grenier K, Dubuc D, Chen T, Artis F, Chretiennot T, Poupot M and Fournie J-J 2013 Recent advances in microwave-based dielectric spectroscopy at the cellular level for cancer investigations *IEEE Trans. Microwave Theory Tech.* **61** 2023–30

Grimnes S and Martinsen Ø G 2010 Alpha-dispersion in human tissue J. Phys.: Conf. Ser. 224 012073

Grimnes S and Martinsen O G 2011 Bioimpedance and Bioelectricity Basics (New York: Academic)

Grimnes S, Rikshospitalet O and Schwan N H P 2002 Interface phenomena and dielectric properties of biological tissue *Encyclopedia Surf.*Colloid Sci. 20 2643–53

Grosse C and Delgado A V 2010 Dielectric dispersion in aqueous colloidal systems Curr. Opin. Colloid Interface Sci. 15 145-59

Grosse C and Schwan H P 1992 Cellular membrane potentials induced by alternating fields Biophys. J. 63 1632-42

Grossi M and Riccò B 2017 Electrical impedance spectroscopy (eis) for biological analysis and food characterization: a review *J. Sens. Sensor Syst.* 6 303–25

Guermazi M, Kanoun O and Derbel N 2014 Investigation of long time beef and veal meat behavior by bioimpedance spectroscopy for meat monitoring *IEEE Sensors J.* 14 3624–30

Harrington RF 1961 Time-Harmonic Electromagnetic Fields (New York: McGraw-Hill) vol 224

Hurt W D 1985 Multiterm Debye dispersion relations for permittivity of muscle *IEEE Transactions on Biomedical Engineering* pp 60–4 Ibba P, Crepaldi M, Cantarella G, Zini G, Barcellona A, Rivola M, Petrelli M, Petti L and Lugli P 2021 Design and validation of a portable ad5933-based impedance analyzer for smart agriculture *IEEE Access* 9 63656–75

Israelachvili J N 2011 Intermolecular and Surface Forces (New York: Academic)

Jackson J D 1998 Classical Electrodynamics (New York: John Wiley & Sons, Inc.)

Jing Y, Jadhao V, Zwanikken J W and Olvera de la Cruz M 2015 Ionic structure in liquids confined by dielectric interfaces *J. Chem. Phys.* 143 194508

Kilic M S, Bazant M Z and Ajdari A 2007a Steric effects in the dynamics of electrolytes at large applied voltages: I. Double-layer charging Phys. Rev. E 75 021502

Kilic M S, Bazant M Z and Ajdari A 2007b Steric effects in the dynamics of electrolytes at large applied voltages: II. Modified poisson-Nernst–Planck equations *Phys. Rev.* E **75** 021503

Koch C 2004 Biophysics of Computation: Information Processing in Single Neurons (Oxford: Oxford University Press)

Kuang W and Nelson S O 1997 Low-frequency dielectric dispersion from ion permeability of membranes J. Colloid Interface Sci. 193 242–9

Kuang W and Nelson S O 1998 Low-frequency dielectric properties of biological tissues: a review with some new insights *Trans. ASAE* 41 173–84

Levin Y 2002 Electrostatic correlations: from plasma to biology Rep. Prog. Phys. 65 1577

Lodi M B et al 2020 A periodic transmission line model for body channel communication IEEE Access 8 160099-115

MaCdonald J R 1970 Double layer capacitance and relaxation in electrolytes and solids Trans. Faraday Soc. 66 943-58

Macdonald J R et al 1987 Impedance Spectroscopy vol 41 (New York: Wiley)

Makarov S N, Noetscher G M and Nazarian A 2015 Low-Frequency Electromagnetic Modeling for Electrical and Biological Systems Using MATLAB (New York: Wiley)

Martinsen \emptyset G, Grimnes S and Karlsen J 1998 Low frequency dielectric dispersion of microporous membranes in electrolyte solution J. Colloid Interface Sci. 199 107–10

Mosher J C, Leahy R M and Lewis P S 1999 EEG and MEG: forward solutions for inverse methods *IEEE Trans. Biomed. Eng.* **146** 245–59 Nordbotten B J, Tronstad C, Martinsen Ø G and Grimnes S 2014 Estimation of skin conductance at low frequencies using measurements at higher frequencies for eda applications *Physiol. Meas.* **35** 1011

Nunez P L et al 2006 Electric Fields of The Brain: The Neurophysics of EEG (USA: Oxford University Press)

Podtaev S, Nikolaev D, Samartsev V, Gavrilov V and Tsiberkin K 2015 Frequency and temperature dependence of skin bioimpedance during a contralateral cold test *Physiol. Meas.* 36 561

Sareni B, Krähenbühl L, Beroual A and Brosseau C 1996 Effective dielectric constant of periodic composite materials *J. Appl. Phys.* 80 1688–96

Schwan H P 1957 Electrical properties of tissue and cell suspensions *Advances in Biological and Medical Physics* vol 5 (Elsevier) pp 147–209 Schwarz G 1962 A theory of the low-frequency dielectric dispersion of colloidal particles in electrolyte solution 1, 2 *J. Phys. Chem.* 66 2636–42

Scott M, Paul R and Kaler K V I S 2000a Theory of frequency-dependent polarization of general planar electrodes with zeta potentials of arbitrary magnitude in ionic media: I. Theoretical foundations and general results *J. Colloid Interface Sci.* 230 377–87

Scott M, Paul R and Kaler K V I S 2000b Theory of frequency-dependent polarization of general planar electrodes with zeta potentials of arbitrary magnitude in ionic media: II. Applications and results from homogeneous and array systems of electrodes *J. Colloid Interface Sci.* 230 388–95

Shilov V N, Delgado A V, Gonzalez-Caballero F and Grosse C 2001 Thin double layer theory of the wide-frequency range dielectric dispersion of suspensions of non-conducting spherical particles including surface conductivity of the stagnant layer *Colloids Surf.* A 192 253–65

Solis F J and Papandreou-Suppappola A 2019 Power dissipation and surface charge in eeg: Application to eigenvalue structure of integral operators *IEEE Trans. Biomed. Eng.* **67** 1232–42

Swaminathan M, Cabrera F S, Pujol J S, Muncuk U, Schirner G and Chowdhury K R 2015 Multi-path model and sensitivity analysis for galvanic coupled intra-body communication through layered tissue *IEEE Trans. Biomed. Circuits Syst.* 10 339–51

Takashima S et al 1989 Electrical Properties of Biopolymers and Membranes (Bristol and Philadelphia: Adam Hilger)

 $Teixeira\ V\ S,\ Krautschneider\ W\ and\ Montero-Rodríguez\ JJ\ 2018\ Bioimpedance\ spectroscopy\ for\ characterization\ of\ healthy\ and\ cancerous\ tissues\ 2018\ IEEE\ Int.\ Conf.\ on\ Electrical\ Engineering\ Photonics\ (EExPolytech)\ (IEEE)\ pp\ 147-51$

Wang H, Tang X, Choy C S and Sobelman G E 2015 Cascaded network body channel model for intrabody communication *IEEE J. Biomed. Health Inform.* **20** 1044–52

Wang M and Pan N 2008 Predictions of effective physical properties of complex multiphase materials Mater. Sci. Eng. R 63 1-30

Wright MR 2007 An Introduction to Aqueous Electrolyte Solutions (Wiley: John Wiley & Sons.)

Zhang Z, Wen L and Jiang L 2018 Bioinspired smart asymmetric nanochannel membranes Chem. Soc. Rev. 47 322-56

Zhbanov A and Yang S 2020 Electrochemical impedance characterization of blood cell suspensions: I. Basic theory and application to twophase systems *IEEE Trans. Biomed. Eng.* **67** 2965–78